Scripta Materialia 238 (2024) 115758

Contents lists available at ScienceDirect

Scripta Materialia

journal homepage: www.journals.elsevier.com/scripta-materialia

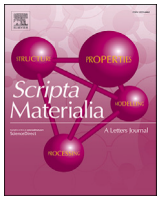

Giant segregation transition as origin of liquid metal embrittlement in the Fe-Zn system

Reza Darvishi Kamachali [a,*], Theophilus Wallis [a], Yuki Ikeda [a], Ujjal Saikia [b], Ali Ahmadian [b], Christian H. Liebscher [b], Tilmann Hickel [a,b], Robert Maaß [a,c]

[a] Federal Institute for Materials Research and Testing (BAM), Unter den Eichen 87, 12205 Berlin, Germany
[b] Max-Planck-Institut für Eisenforschung GmbH, Max-Planck-Straße 1, 40237 Düsseldorf, Germany
[c] Department of Materials Science and Engineering, University of Illinois at Urbana-Champaign, Urbana, 61801 Illinois, USA

ABSTRACT

A giant Zn segregation transition is revealed using CALPHAD-integrated density-based modeling of segregation into Fe grain boundaries (GBs). The results show that above a threshold of only a few atomic percent Zn in the alloy, a substantial amount of up to 60 at.% Zn can segregate to the GB. We found that the amount of segregation abruptly increases with decreasing temperature, while the Zn content in the alloy required for triggering the segregation transition decreases. Direct evidence of the Zn segregation transition is obtained using high-resolution scanning transmission electron microscopy. Base on the model, we trace the origin of the segregation transition back to the low cohesive energy of Zn and a miscibility gap in Fe-Zn GB, arising from the magnetic ordering effect, which is confirmed by ab-initio calculations. We also show that the massive Zn segregation resulting from the segregation transition greatly assists with liquid wetting and reduces the work of separation along the GB. The current predictions suggest that control over Zn segregation, by both alloy design and optimizing the galvanization and welding processes, may offer preventive strategies against liquid metal embrittlement.

Liquid Metal Embrittlement (LME) is a major safety concern in structural engineering. For Zn-coated steels, LME leads to severe limitations in manufacturing and related designs in the automotive industry [1,2]. Extensive research has been devoted to understanding the underlying mechanisms of LME (see for instance [3–5] and references therein). Embedded in several analyses, wetting of grain boundaries (GBs) has been proposed as a leading mechanism in promoting crack initiation and propagation in Zn welding regions [6,7]. The extent and significance of wetting are argued to depend on the solubility of the embrittling metal in the base alloy [8]. Another mechanism repeatedly discussed for LME is stress-assisted diffusion, promoting the formation of a Zn-penetration-zone and thus cracking [9,10]. Recently, it has also been proposed that LME can be driven by the formation of brittle Zn-rich Γ precipitates that further create stress heterogeneities in the uncracked GBs [11].

As a common point of departure in various mechanisms, the interaction between Zn and Fe atoms at GBs is of fundamental importance: In particular, one can ask if, prior to wetting or GB precipitation, the segregation of Zn could play a critical role on a much smaller scale? Indeed, careful investigations revealed that Zn-rich precipitates form along the GB far ahead of the crack tip [11,12]. Furthermore, atom probe tomography has revealed significant elemental segregation along GBs [13]. These observations brace Zn segregation as a *precursor* for LME, weakening the GB and accelerating interfacial wetting and precipitation prior to crack initiation. Even for the mechanism of stress-assisted diffusion, the enlargement of the so-called Zn-penetration-zone should be studied in conjunction with the GBs' segregation response. For these reasons and because of its potential for preventive design against LME, it is highly desirable to explore and understand Zn segregation and related GB phase behavior.

In the bulk Fe-Zn phase diagram, the BCC solid solution shows a miscibility gap over a significant range of temperatures and compositions, see Fig. S1 in the Supplementary Material (SM). Although often neglected in the usual Fe-Zn phase diagram (due to the assumption of an equilibrium formation of the Zn-rich Γ phase), this miscibility gap has important implications for the Zn segregation behavior: In fact, the presence of such a miscibility gap can lead to a segregation transition phenomenon as demonstrated in other alloy systems [14–16]. Furthermore, due to the small cohesive energy of Zn, the driving force for any Zn segregation is expected to be high, i.e., the energy of an Fe GB can be dramatically reduced with Zn segregation. To capture these two major features, density-based Gibbs free energy formalism for describing GBs is considered [14]:

* Corresponding author.
E-mail address: reza.kamachali@bam.de (R. Darvishi Kamachali).

https://doi.org/10.1016/j.scriptamat.2023.115758
Received 12 May 2023; Received in revised form 31 August 2023; Accepted 5 September 2023
Available online 18 September 2023

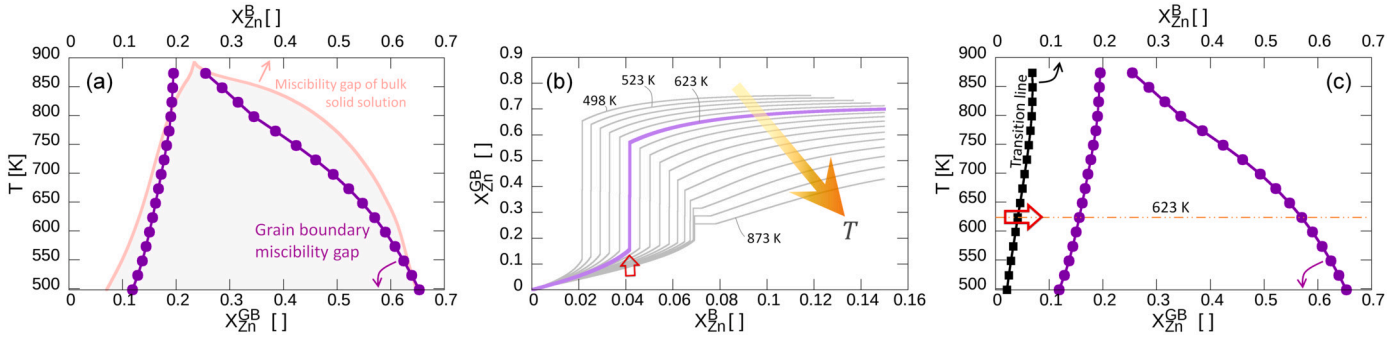

Fig. 1. Grain boundary (GB) phase diagram. (a) The GB miscibility gap (circles) computed utilizing the CALPHAD-integrated density-based method. Thermo-Calc TCFE11 database was used. The miscibility gap of the parent α (BCC) bulk phase is shown for comparison in the background. The superscripts B and GB refer to bulk and grain boundary compositions, respectively. (b) GB segregation isotherms computed for various temperatures using CALPHAD-integrated density-based method. The abrupt jump in each isotherm indicates the segregation transition. (c) The complete density-based GB phase diagram is obtained, combining the results in panels (a) and (b). At each given temperature, the *transition line* (squares) marks the critical alloy (bulk) composition at which the segregation transition occurs. A massive Zn segregation transition is predicted for alloy compositions and temperatures changing from the left to the right side of the transition line. The segregation transition at $T = 623$ K is marked, as an example, to link the results in panels (b) and (c). (For interpretation of the colors in the figure(s), the reader is referred to the web version of this article.)

$$G(T,\rho,X_{Zn}) = X_{Fe}G_{Fe}(T,\rho) + X_{Zn}G_{Zn}(T,\rho) + \rho^2\Delta H^B\left(T,X_{Zn}\right) - T\Delta S^B\left(T,X_{Zn}\right) \quad (1)$$

with $G_i(T,\rho) = \rho^2 E_i^B + \rho\left(G_i^B(T) - E_i^B\right)$. Here, the dimensionless atomic density ρ defines the parent bulk phase when $\rho = 1$ or a GB when $\rho < 1$.

All other terms are bulk thermodynamic properties available from CALPHAD databases: The Gibbs free energy G_i^B and potential energy E_i^B of the pure i substance, the mixing enthalpy ΔH^B and the mixing entropy ΔS^B —the superscript B denotes bulk properties throughout this paper. Compared to its original formulation [14], in this study, we omit the gradient energy contributions in the free energy and, instead, focus on the temperature and composition dependence of the Zn segregation phenomenon.

The density-based approach has been successfully applied for microstructure and alloy design in a broad range of materials [17–21]. The key strength of this method is its natural capacity to be integrated with the CALPHAD framework and atomistic simulations, providing in-depth multi-scale insights into the phase behavior of GBs. We study a prototypical GB with $\rho = 0.92$ motivated by atomistic simulations of BBC-Fe GBs. For the calculations, we use the Thermo-Calc TCFE11 database. The computational details and input parameters are given in Appendix A and B in the SM.

Fig. 1(a) shows the computed GB miscibility gap (solid lines with circles). Compared to the parent bulk phase (red curve in the background), the GB miscibility gap slightly shrinks and shifts, however, it still covers a broad range of temperatures and compositions. Applying the equal chemical potential condition [14], one can study the coexistence of the GB and bulk. This gives the segregation isotherms shown in Fig. 1(b). The isotherms reveal a segregation transition, i.e., an abrupt increase (jump) in the GB Zn segregation with increasing Zn content in the bulk solid solution. This corresponds to the miscibility gap of the GB. We found that the amount of Zn in the GB massively increases during the segregation transition, markedly exceeding the previously observed large segregation transitions in iron alloys [15]. For instance, at $T = 623$ K, about 60 at.% Zn segregate to the GB if only 4 at.% of Zn are added to BCC-Fe.

The critical alloy compositions, corresponding to the segregation transitions, can be obtained from segregation isotherms, i.e., the solid black line with squares in the left corner in Fig. 1(c), referred to as the *transition line*. With this critical information, the GB phase diagram is complete: Fig. 1(c) illustrates that for alloy compositions and temperatures to the left side of the transition line, low segregation of Zn to the GB is expected. In contrast, shifting to the right side of the transition line induces massive Zn segregation, in which the GB composition dramatically increases, crossing its own miscibility gap. This corresponds to the high-segregation branch in the segregation isotherms, Fig. 1(b). The results in Figs. 1(b) and (c) show that the magnitude of the segregation transition (the height of the jump) and the degree of segregation significantly increase with decreasing the temperature. Such low temperatures and temperature decreases can occur during the cooling stages in galvanization and welding processes.

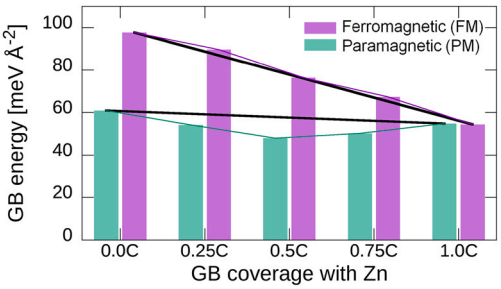

Fig. 2. GB energy from DFT calculations. The energy of a Σ5 [100](013) GB is computed for various levels of Zn coverage (C: coverage), with and without the magnetic ordering effect. The black curves connect the GB energies for the end-members with no and full coverage. In the paramagnetic state, Zn favorably dissolves in the GB (convex) while in the ferromagnetic state, the GB shows a miscibility gap (concave).

The origin of the miscibility gap in the Fe-Zn bulk system has been attributed to a magnetic ordering effect, i.e., the presence of different magnetic states [22,23]. Using the density-based thermodynamic approach, here we show that this magnetic miscibility gap of the bulk is inherited by the GB and plays a central role in governing the segregation transition. To verify the existence of such a magnetic miscibility gap for GBs, we have performed DFT calculations of Zn segregation in a Σ5 GB, with and without the consideration of magnetic disorder. The computational details are given in Appendix C in the SM. Fig. 2 reveals that the strong segregation for Zn to GBs discussed in previous DFT calculations [24,25] is only present in the ferromagnetic case. Without magnetic ordering (paramagnetic state), the segregation of Zn only reduces the GB energy up to a coverage of 50%, i.e., the energy curve is convex. In the presence of a magnetic ordering (ferromagnetic state), the GB shows a concave energy curve, indicating that the Zn-segregated GB becomes thermodynamically unstable. This demonstrates that the miscibility gap due to the magnetic ordering effect is inherited by the GB; thus, above a certain composition, the GB prefers to decompose into Zn-rich and Zn-poor segments, confirming the results of density-based model.

In fact, recent studies have revealed that such chemical decomposition at the GB is direct evidence of a segregation transition [15,20].

To examine this for the Fe-Zn system, we performed high-resolution transmission electron microscopy of a Σ5 GB in a Zn-coated BCC-Fe bicrystal. Fig. 3(a) shows a HAADF scanning transmission micrograph and the corresponding STEM-EDS elemental Zn map and line profile for the GB. Experimental details are given in Appendix D in the SM. We found that with only 5 at.% Zn in the bulk, the Zn strongly segregates to the GB and decomposes into rich and poor patches. The existence of the Zn patches along the GB reveals an interfacial phase decomposition, as previously demonstrated [15,20], and confirms the existence of the segregation transition in the Fe-Zn system. The concentration of Zn patches reaches 40 at.% which is in the range of predicted values in Fig. 1(b). We note that an additional effect of gradient energy terms is neglected in the current calculations that can be responsible for the spread of Zn in the grain boundary region in Fig. 3(b). Co-segregation with other elements is also evidenced to reduce the Zn segregation at the GB [26]. The cross-validations from the DFT calculations and the experiment confirm the density-based modeling predictions of the segregation transition in the Fe-Zn system.

Given the complex temperature profiles experienced during the processing of Zn-coated steels [27], the alloy compositions and experienced temperatures fall easily beyond the transition line in the GB phase diagram (Fig. 1(c)). Once the Zn supply into the alloy is available via diffusion into the grain interior, the GB segregation transition can be triggered. This can also happen during the cooling stage, as the required amount of Zn in the grain to trigger the segregation transition is low and further decreases with decreasing the temperature. The experimental results shown in Fig. 3(a) reveal such segregation transition occurring during the cooling after a heat treatment process. Interestingly, our calculations show that the Zn segregation becomes much stronger with decreasing the temperature.

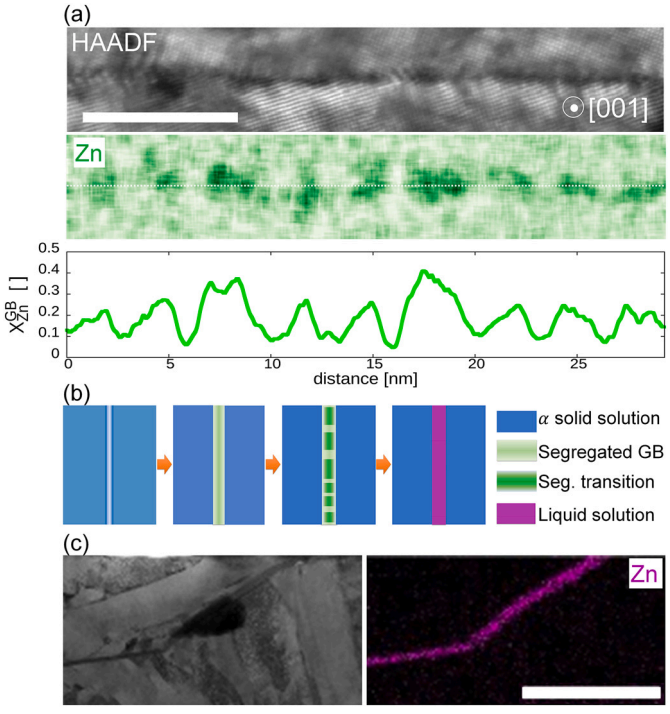

Fig. 3. GB segregation transition and related wetting. (a) High-angle annular dark-field (HAADF) imaging in the scanning transmission electron microscope (STEM) showing a Σ5 GB (scale bar 7 nm). Both grains are oriented along the [001] axis. The corresponding elemental Zn map and line profile along the GB, obtained by STEM energy dispersive spectroscopy (STEM-EDS), reveal interfacial spinodal decomposition with localized Zn-rich patches, which is the signature of a segregation transition. (b) Schematic sequence of a segregation transition assisting the formation of the liquid phase in the GB. (c) Bright-field scanning transmission micrograph (scale bar 1 μm) evidencing Zn-rich wetting along a GB after a spot welding process. Further experimental details are given in Appendix D in the SM.

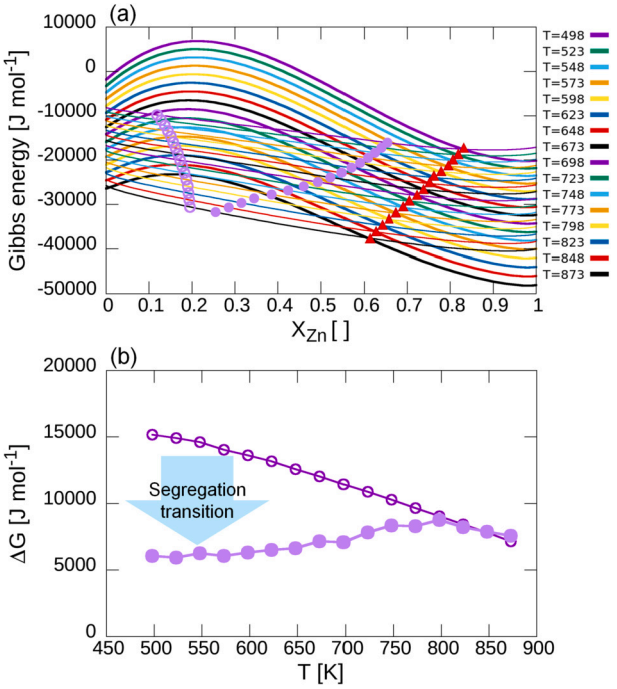

Fig. 4. Segregation-induced liquid formation at the GB. (a) Free energies of GB (thin curves) and liquid Fe-Zn solution (thick curves) for different temperatures. The intersections of two free energy curves are also marked with triangles. For GB compositions beyond the intersection point, the liquid phase becomes stable, i.e., $\Delta G < 0$. GB compositions right before and after the segregation transition are marked on the GB free energy curves with unfilled and filled circles, respectively. (b) ΔG as a function of temperature are shown for the two sets of GB compositions marked in panel (a). The same markers are used as in panel (a). The arrow in panel (b) indicates that the massive segregation transition dramatically decreases the barrier for the formation of the liquid phase from segregated GBs.

The significant amount of Zn in the GB, originating from the segregation transition, can dramatically affect the course of GB wetting, as schematically shown in Fig. 3(b). Experimentally, we observed this in the welding process of a steel specimen, giving the thick Zn solution layer shown in Fig. 3(c). Although the segregation might not be the sole origin of wetting (e.g. stresses may play a significant role), the segregation transition is expected to dramatically boost it. To understand this influence, we studied the barrier for the formation of the liquid phase from a Zn-enriched GB, $\Delta G = G^L - G^{GB}$. Here the free energies of the liquid solution $G^L(T, X_{Zn})$ and the segregated GB, $G^{GB} = G(\rho = 0.92, T, X_{Zn})$ are obtained from CALPHAD database TCFE11 and through Eq. (1), respectively.

Fig. 4(a) shows the free energies of the GB and the liquid solution for various temperatures. The intersections of the two free energies corresponding to $\Delta G = 0$ are marked (triangles). On the GB free energies, we also marked the GB compositions at the segregation transition, and the low and high values at the jump (circles). We computed ΔG values for these two sets of GB compositions to specifically reveal the effect of segregation transition. Fig. 4(b) reveals that the barrier for the formation of the liquid phase significantly increases with a decrease in the temperature. The results show that both compositional and energetic barriers for the formation of the liquid phase are greatly reduced by the Zn segregation transition. Further applying the density-based model for intermetallic phases, we found that the segregation transition enables the formation of the Zn-rich Γ phase ahead of the crack tip. This is thoroughly discussed in Ref. [12].

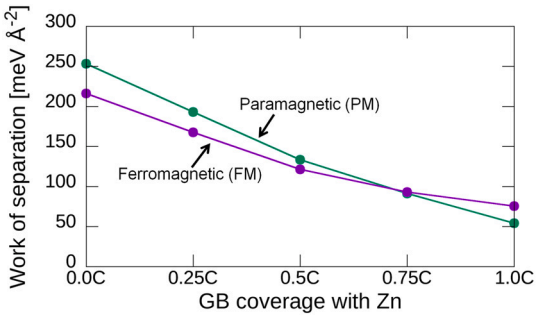

Fig. 5. GB's work of separation. The work of separation of a Σ5 [100](013) GB for various levels of coverage with Zn, with and without magnetic ordering effect.

Prior to the liquid formation, the massive Zn segregation can also have great significance for promoting an easy crack initiation by weakening the GB. We studied the work of separation of a Σ5 GB as a function of Zn coverage, using DFT calculations. The results in Fig. 5 show that the segregation of Zn dramatically reduces the GB's work of separation. These confirm the results from previous works [24–26]. We found that compared to the paramagnetic state, the GB exhibits a slightly reduced work of separation and weaker dependence on the Zn content in the ferromagnetic state. Nevertheless, in both cases the overall reduction in the work of separation is significant. In fact, for 50% Zn coverage, the work of separation for the GB reduces almost by half. These results suggest that once the Zn segregation transition occurs, GB weakens dramatically. Such a weakened GB ahead of a crack tip is highly prone to opening, thus promoting embrittlement in the material.

To summarize, we reveal and explain a giant segregation transition occurring during Zn segregation into Fe GBs using CALPHAD-integrated density-based modeling. Two central insights of the model are that it shows the GB in the Fe-Zn system can have a large miscibility gap and this is of a magnetic origin. The magnetic origin of GB miscibility gap is also confirmed by DFT calculations. The segregation transition is evidenced by our HAADF-STEM exprimental measurements, revealing an interfacial phase decomposition (formation of Zn-rich patches) along GB. Our results shed light on the origin and mechanisms of LME in Zn-coated steels and its strong dependence on temperature and alloy composition. In particular, we found that the amount of segregation dramatically increases with decreasing the temperature, while the required amount of Zn in the alloy to trigger the segregation transition decreases. These emphasize the significance of the cooling stage during processing. We show that the segregation transition markedly assists with the formation of an interfacial liquid phase and weakens the GB by reducing the work of separation. The strong temperature and composition dependence of the Zn segregation transition implies that LME in the Fe-Zn system should be preventable via alloy and processing design strategies that suppress the revealed segregation transition. Follow-up density-based phase-field simulations and guided experiments are planned to explore the detailed influence of alloying and processing parameters.

CRediT authorship contribution statement

RDK conceived the idea and the collaborations, conducted the thermodynamic calculations, supervised grain boundary density calculations and wrote the manuscript. TW computed the grain boundary density from atomistic simulations. US conducted the ab initio calculations. AA conducted the experiments on the bicrystal specimen. YI conducted the experiments on the welding specimen. TH supervised the ab initio calculations and revised the manuscript. CHL supervised the experiments on the bicrystal specimen and revised the manuscript. RM supervised the experiments on the welding specimen and revised the manuscript. All authors reviewed and edited the manuscript. RDK, CHL, TH and RM secured funding.

Declaration of competing interest

The authors declare that they have no known competing financial interests or personal relationships that could have appeared to influence the work reported in this paper.

Data availability

Further data and codes of this study are available from the corresponding author.

Acknowledgements

RDK acknowledges the financial support from the German Research Foundation (DFG) within the project *DA 1655/3-1* and the Heisenberg program's project *DA 1655/2-1*. US and TH acknowledge the DFG support within the transfer project T07 of the *SFB761* "Stahl - ab initio". CHL acknowledges the DFG support within the project *LI 2133/7-1*. YI gratefully acknowledges the Takenaka Overseas Scholarship Foundation for their kind support of his graduate work. This research was carried out in part at the electron microscopy center at BAM.

Appendix A. Supplementary material

Supplementary material related to this article can be found online at https://doi.org/10.1016/j.scriptamat.2023.115758.

References

[1] R. Sierlinger, M. Gruber, A cracking good story about liquid metal embrittlement during spot welding of advanced high strength steels, White Paper, voestalpine Stahl GmbH, Linz, Austria, 2017.
[2] D. Bhattacharya, Liquid metal embrittlement during resistance spot welding of Zn-coated high-strength steels, Mater. Sci. Technol. 34 (2018) 1809.
[3] B. Joseph, M. Picat, F. Barbier, Liquid metal embrittlement: a state-of-the-art appraisal, Eur. Phys. J. Appl. Phys. 5 (1999) 19.
[4] K. Nilsson, A. Hojna, Overview of mechanisms & models for liquid metal embrittlement and future directions, EU Science Hub-European Commission, 450, 2018.
[5] M. Razmpoosh, C. DiGiovanni, Y. Zhou, E. Biro, Pathway to understand liquid metal embrittlement (LME) in Fe-Zn couple: from fundamentals toward application, Prog. Mater. Sci. 121 (2021) 100798.
[6] K. Wolski, V. Laporte, N. Marie, M. Biscondi, About the importance of nanometer-thick intergranular penetration in the analysis of liquid metal embrittlement, Interface Sci. 9 (2001) 183.
[7] V.S.P.K. Bhogireddy, Liquid metal induced grain boundary embrittlement, Ph.D. thesis, Ruhr-University Bochum, 2016.
[8] F.A. Shunk, W.R. Warke, Specificity as an aspect of liquid metal embrittlement, Scr. Metall. 8 (1974) 519.
[9] Z. Ling, M. Wang, L. Kong, K. Chen, Towards an explanation of liquid metal embrittlement cracking in resistance spot welding of dissimilar steels, Mater. Des. 195 (2020) 109055.
[10] C. DiGiovanni, A.G. Kalashami, E. Biro, N. Zhou, Liquid metal embrittlement transport mechanism in the Fe/Zn system: stress-assisted diffusion, Materialia 18 (2021) 101153.
[11] Y. Ikeda, R. Yuan, A. Chakraborty, H. Ghassemi-Armaki, J. Zuo, R. Maaß, Early stages of liquid-metal embrittlement in an advanced high-strength steel, Mater. Today Adv. 13 (2022) 100196.
[12] Y. Ikeda, H. Ni, A. Chakraborty, H. Ghassemi-Armaki, J. Zuo, R. Darvishi Kamachali, R. Maaß, Segregation-induced grain-boundary precipitation during early stages of liquid-metal embrittlement of an advanced high-strength steel, Acta Mater. 119243 (2023).
[13] M. Razmpoosh, B. Langelier, E. Marzbanrad, H. Zurob, N. Zhou, E. Biro, Atomic-scale investigation of liquid-metal-embrittlement crack-path: revealing mechanism and role of grain boundary chemistry, Acta Mater. 204 (2021) 116519.
[14] R. Darvishi Kamachali, A model for grain boundary thermodynamics, RSC Adv. 10 (2020) 26728.
[15] R. Darvishi Kamachali, A. Kwiatkowski da Silva, E. McEniry, D. Ponge, B. Gault, J. Neugebauer, D. Raabe, Segregation-assisted spinodal and transient spinodal phase separation at grain boundaries, npj Comput. Mater. 6 (2020) 191.
[16] L. Wang, R. Darvishi Kamachali, Density-based grain boundary phase diagrams: application to Fe-Mn-Cr, Fe-Mn-Ni, Fe-Mn-Co, Fe-Cr-Ni and Fe-Cr-Co alloy systems, Acta Mater. 116668 (2021).
[17] L. Li, R. Darvishi Kamachali, Z. Li, Z. Zhang, Grain boundary energy effect on grain boundary segregation in an equiatomic high-entropy alloy, Phys. Rev. Mater. 4 (2020) 053603.

[18] L. Wang, R. Darvishi Kamachali, Incorporating elasticity into CALPHAD-informed density-based grain boundary phase diagrams reveals segregation transition in Al-Cu and Al-Cu-Mg alloys, Comput. Mater. Sci. 199 (2021) 110717.
[19] X. Zhou, R. Darvishi Kamachali, B.L. Boyce, B.G. Clark, D. Raabe, G.B. Thompson, Spinodal decomposition in nanocrystalline alloys, Acta Mater. 215 (2021) 117054.
[20] T. Wallis, R. Darvishi Kamachali, Grain boundary structural variations amplify segregation transition and stabilize co-existing spinodal interfacial phases, Acta Mater. 242 (2023) 118446.
[21] L. Wang, R. Darvishi Kamachali, Calphad integrated grain boundary co-segregation design: towards safe high-entropy alloys, J. Alloys Compd. 933 (2023) 167717.
[22] G. Reumont, P. Perrot, J. Fiorani, J. Hertz, Thermodynamic assessment of the Fe-Zn system, J. Phase Equilib. 21 (2000) 371.
[23] X. Su, N.-Y. Tang, J.M. Toguri, Thermodynamic evaluation of the Fe–Zn system, J. Alloys Compd. 325 (2001) 129.
[24] K.-D. Bauer, M. Todorova, K. Hingerl, J. Neugebauer, A first principles investigation of zinc induced embrittlement at grain boundaries in bcc iron, Acta Mater. 90 (2015) 69.
[25] D. Scheiber, K. Prabitz, L. Romaner, W. Ecker, The influence of alloying on Zn liquid metal embrittlement in steels, Acta Mater. 195 (2020) 750.
[26] A. Ahmadian, D. Scheiber, X. Zhou, B. Gault, L. Romaner, R. Darvishi Kamachali, W. Ecker, G. Dehm, C.H. Liebscher, Interstitial segregation has the potential to mitigate liquid metal embrittlement in iron, Adv. Mater. 2211796 (2023).
[27] Z. Hou, I.-S. Kim, Y. Wang, C. Li, C. Chen, Finite element analysis for the mechanical features of resistance spot welding process, J. Mater. Process. Technol. 185 (2007) 160.